General Psychiatry

Presurgical structural imaging and clinical outcome in combined bed nucleus of the stria terminalis–nucleus accumbens deep brain stimulation for treatment-resistant depression

Fengting Wang ![ORCID] ,[1] Lulin Dai,[1,2] Tao Wang,[1] Yingying Zhang,[1,3] Yuhan Wang,[1] Yijie Zhao,[3,4] Yixin Pan,[1] Liuguan Bian,[1] Dianyou Li,[1] Shikun Zhan,[1] Yijie Lai ![ORCID] ,[1] Valerie Voon,[3,5] Bomin Sun[1]

For numbered affiliations see end of article.

Correspondence to
Professor Bomin Sun;
sbm11224@rjh.com.cn

Professor Valerie Voon;
vv247@cam.ac.uk

Dr Yijie Lai;
laiyijie0901@sjtu.edu.cn

ABSTRACT

Background Structural imaging holds great potential for precise targeting and stimulation for deep brain stimulation (DBS). The anatomical information it provides may serve as potential biomarkers for predicting the efficacy of DBS in treatment-resistant depression (TRD).

Aims The primary aim is to identify preoperative imaging biomarkers that correlate with the efficacy of DBS in patients with TRD.

Methods Preoperative imaging parameters were estimated and correlated with the 6-month clinical outcome of patients with TRD receiving combined bed nucleus of the stria terminalis (BNST)–nucleus accumbens (NAc) DBS. White matter (WM) properties were extracted and compared between the response/non-response and remission/non-remission groups. Structural connectome was constructed and analysed using graph theory. Distances of the volume of activated tissue (VAT) to the main modulating tracts were also estimated to evaluate the correlations.

Results Differences in fibre bundle properties of tracts, including superior thalamic radiation and reticulospinal tract, were observed between the remission and non-remission groups. Distance of the centre of the VAT to tracts connecting the ventral tegmental area and the anterior limb of internal capsule on the left side varied between the remission and non-remission groups (p=0.010, t=3.07). The normalised clustering coefficient (γ) and the small-world property (σ) in graph analysis correlated with the symptom improvement after the correction of age.

Conclusions Presurgical structural alterations in WM tracts connecting the frontal area with subcortical regions, as well as the distance of the VAT to the modulating tracts, may influence the clinical outcome of BNST–NAc DBS. These findings provide potential imaging biomarkers for the DBS treatment for patients with TRD.

WHAT IS ALREADY KNOWN ON THIS TOPIC

⇒ Structural alterations are shown to have an impact on deep brain stimulation (DBS) efficacy.

WHAT THIS STUDY ADDS

⇒ This is the first study demonstrating presurgical structural features that influence the outcome of patients with treatment-resistant depression (TRD) receiving combined bed nucleus of the stria terminalis (BNST)–nucleus accumbens (NAc) DBS. White matter integrity of tracts connecting the frontal area with subcortical regions and the distance of the volume of activated tissue to the ventral tegmental area-anterior limb of internal capsule tract can play a role in DBS modulation in patients with TRD.

HOW THIS STUDY MIGHT AFFECT RESEARCH, PRACTICE OR POLICY

⇒ This study provided potential imaging biomarkers for outcome prediction of combined BNST–NAc DBS and helped in understanding the underlying mechanisms of DBS modulation.

disability, with over 30% of patients experiencing treatment resistance.[1] Patients with treatment-resistant depression (TRD) are refractory to conventional psychotherapeutic strategies, while deep brain stimulation (DBS) may exert long-lasting and better efficacy.[2] However, various clinical trials with different DBS targets have reported substantial variabilities in individual response to DBS, with some patients achieving complete remission after DBS while others exhibiting poor response, highlighting the need for outcome prediction in patient management.[2] DBS targets, including ventral capsule/ventral striatum, ventral anterior limb of the internal capsule, bed nucleus of the stria

INTRODUCTION

Major depressive disorder is a global public health concern and the leading cause of

terminalis (BNST) and nucleus accumbens (NAc), are anatomically close to each other and interconnected by dense fibre tracts, the stimulation of which is reported to modulate overlapping yet differentiated pathways that may share a cooperative functionality.[3] We hypothesised that combined stimulation of these targets may synergistically exert the therapeutic effect, and therefore targeted the BNST–NAc region.

Structural imaging is a prerequisite step in functional neurosurgery. It provides anatomical information required for targeting and can illustrate chronic treatment-related structural alterations. Differences in fibre properties have been shown to correlate with DBS outcomes in conditions such as Parkinson's disease and obsessive–compulsive disorder.[45] In the treatment of TRD, frontal volumes and frontal white matter (WM) structure were reported to correlate with the DBS outcome of the superolateral medial forebrain bundle (slMFB).[6] A large profile of WM tracts, especially tracts connecting the medial frontal area, was associated with DBS response in patients who received subcallosal cingulate cortex DBS.[7] Nevertheless, these results have not been replicated. The prediction of DBS outcome using preoperative neuroimaging features remains unexplored in the combined BNST–NAc DBS for TRD.

Major depressive disorder is hypothesised to be a disconnection syndrome in which connectivity between hub regions in brain circuits is impaired, leading to an imbalance of emotional circuitry.[8] In this study, we evaluated preoperative structural brain connectivity, including the main fibre tracts connecting cortical and subcortical regions, as well as the brain connectome using graph analysis in patients with TRD. Our goal is to identify preoperative imaging biomarkers that predict the efficacy of DBS in patients with TRD.

METHOD

Participants

Patients with TRD who were considered for neurosurgery at Ruijin Hospital from April 2021 to December 2022 were recruited for the imaging study. Among the 23 patients who underwent surgery, 8 patients without diffusion-weighted imaging (DWI) results were excluded from the analysis. One patient was excluded due to poor imaging quality. A total of 14 patients were enrolled in the analysis (figure 1). Detailed inclusion and exclusion criteria for patients with TRD eligible for neurosurgery are described in online supplemental file 1.

Surgical procedure and clinical assessment

Electrodes were implanted bilaterally in the dual target region of BNST and NAc using stereotactic frame-based magnetic resonance technique using SR1202-S 8-contact leads (8 contacts of 1.5 mm with a spacing of 0.5 mm; SceneRay, Suzhou, China).[9] The details of the procedure have been previously described.[10]

Clinical outcomes were measured using the 17-item Hamilton Depression Rating Scale (HAMD-17),[11] the Montgomery-Asberg Depression Rating Scale 20[12] and the 14-item Hamilton Anxiety Rating Scale (HAMA-14).[13] The assessments were conducted presurgically and postsurgically at each programming session. Other examiner-rating or self-reported scales were also collected at
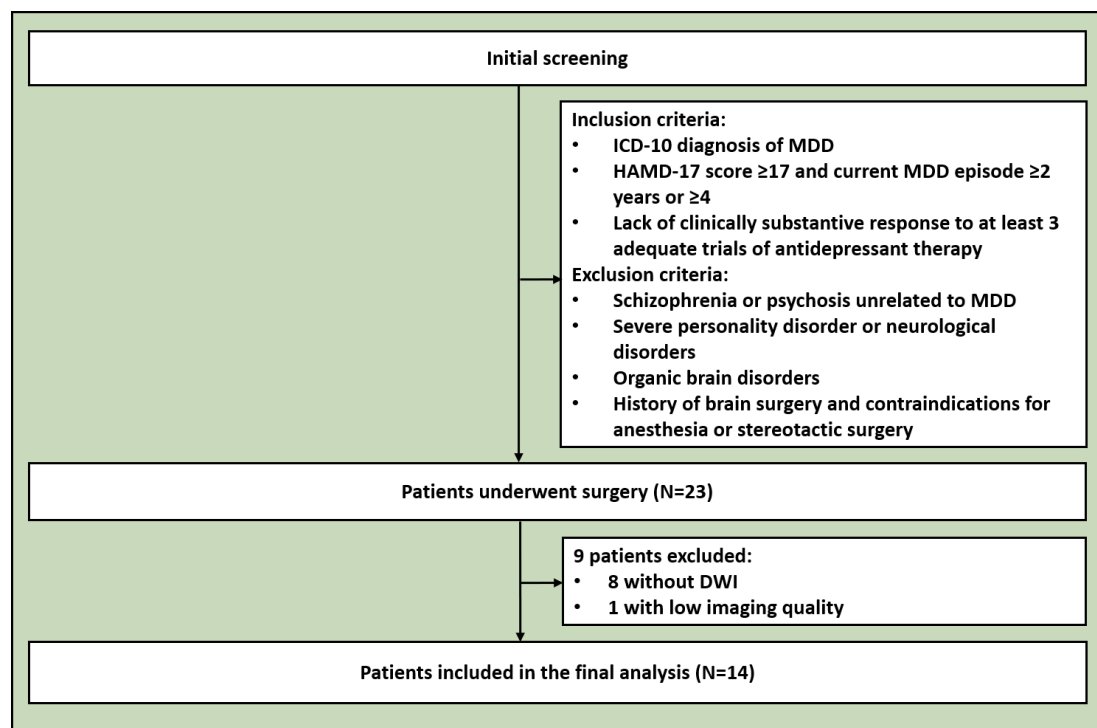
Figure 1 Flowchart of patient screening and inclusion. DWI, diffusion-weighted imaging; HAMD, Hamilton Depression Rating Scale; ICD, International Classification of Diseases; MDD, major depressive disorder.

baseline, including the Depression and Somatic Symptoms Scale (DSSS),[14] the 16-item Quick Inventory of Depressive Symptomatology self-report,[15] the Sheehan Disability Scale (SDS),[16] the Medical Outcomes Study 36-Item Short Form Health Survey (SF-36),[17] the Barratt Impulsiveness Scale-11 (BIS-11)[18] and the Dimensional Anhedonia Rating Scale (DARS).[19] The criteria for response and remission were ≥50% reduction of HAMD-17 Score from baseline and HAMD Score ≤7, respectively.

Postoperative programming scheme has been described in a previous study.[10] An initial programming session 1 week after surgery was launched to assess the efficacy and safety of each electrode contact. Experienced psychiatrists and neurosurgeons tested each contact individually through careful parameter titration with monopolar stimulation. Amplitude was gradually increased in 0.5 V steps from 2.0 to 6.0 V with fixed frequency (130 Hz) and pulse width (90 μs) for 30–60 s, except when any acute adverse effects were observed. If little clinical improvement was achieved, we tested voltages greater than 6.0 V and adjustments in pulse width and frequency. Induction of beneficial effects or adverse effects was documented. Follow-up programming was based on the subject's experience feedback and scale evaluation.

Image acquisition
Preoperative imaging was performed on a 3T MRI system (Magnetom Prisma, Siemens, Erlangen, Germany). Axial three-dimensional T1-weighted Turbo-Field-Echo sequence was acquired with the following specifications: TR/TE 3000/2.56 ms, voxel size $0.8 \times 0.8 \times 0.8$ mm^3, field of view (FOV) 256×256 mm^2. DWI images were acquired using a single-shot, spin-echo echo planar imaging sequence with 30 diffusion directions of b=1500 s/mm^2, 60 diffusion directions of b=3000 s/mm^2 and 11 interspersed scans of b=0 s/mm^2 along AP direction. Scans with b=0 s/mm^2 along PA direction were also acquired for the correction of susceptibility-induced distortions. The other specifications include TR/TE 6800/75 ms, voxel size $1.5 \times 1.5 \times 1.5$ mm^3 and FOV 192×192 mm^2.

Electrode reconstruction and volume of activated tissue (VAT) estimation
DBS electrodes were localised using Lead-DBS (http://www.lead-dbs.org) and the PaCER algorithm. In brief, postoperative CT images were first linearly coregistered to preoperative MRI and normalised into ICBM 2009b NLIN asymmetric space using the SyN approach implemented in Advanced Normalisation Tools (ANTs). DBS electrodes were then localised using Lead-DBS and warped into the MNI space using the PaCER algorithm after visual review and refinement of the coregistration and normalisation.[20]

To construct a volume conductor model of the DBS electrode and surrounding tissue, a tetrahedral volume mesh was generated based on the surface mesh of DBS electrodes and subcortical nuclei using the Iso2Mesh toolbox (http://iso2mesh.sourceforge.net).

Conductivities of 0.33 S/m and 0.14 S/m were assigned to grey matter (GM) and WM, respectively. Based on the volume conductor model, the potential distribution was simulated using the integration of the FieldTrip-SimBio pipeline into Lead-DBS (https://www.mrt.uni-jena.de/simbio/index.php/; http://fieldtriptoolbox.org). In case of monopolar stimulation, the surface of the volume mesh served as the anode. Subsequently, the gradient of the potential distribution was calculated by derivation of the finite element method solution. The gradient was thresholded for magnitudes above a commonly used value of 0.2 V/mm to define the VAT.

Tractography and microstructural measures
Motion, eddy current and susceptibility-induced distortion corrections were processed using FSL V.6.0 (FMRIB Software Library).[21] The multishell diffusion data were then reconstructed in DSI studio using generalised q-sampling imaging[22] with a diffusion sampling length ratio of 1.25. The normalised quantitative anisotropy (NQA), fraction anisotropy (FA), mean diffusivity (MD), axial diffusivity (AD) and radial diffusivity (RD) maps were derived for each participant. A deterministic fibre tracking algorithm[23] was used with a step size of 0.5 mm, an NQA threshold of 0.02, a change threshold of 20% and an angular threshold of 60°. Tracks with length shorter than 30 or longer than 300 mm were discarded. A total of 1 000 000 seeds were placed at the whole brain and at the VAT estimated in the previous step registered to the native space by DSI studio. Automated fibre tracking was conducted to recognise and cluster the tracts based on the HCP tractography atlas.[24] Mean fibre features of tracts were then extracted for each subject for statistical analysis. Percentage of fibre tracts traversing the VAT was calculated by dividing the number of specific fibre tracts by the total number of fibre tracts recognised in tracts traversing the VAT.

Tract-based spatial statistics (TBSS) was used to conduct the voxel-wise statistical analysis.[25] All subjects' FA data were aligned to an FMRIB58-FA_1 mm template in MNI space in a non-linear registration calculation method. The mean FA image of all subjects was created. Voxels with FA value threshold of 0.2 were abstracted to establish average FA images and average FA skeleton images. The standard space FA images of each subject were projected onto their average FA skeleton images and generated individual FA skeleton images, respectively. The NQA, AD, RD and MD skeleton images were also calculated based on FA skeleton images. Finally, a randomise tool was used to analyse the whole-brain non-parametric statistical values between groups, and a total of 5000 permutations were performed for each contrast. The p value images, which were corrected by threshold-free cluster enhancement, were thresholded at 0.05. Age was used as a covariate.

Distance estimation
Distances of the centre of the VAT to the anterior thalamic radiation and tracts connecting the ventral

tegmental area (VTA) to the anterior limb of internal capsule (ALIC) as a reference of slMFB were calculated.[26 27] The left/right anterior thalamic radiation was built using the automated fibre tracking algorithm in DSI studio. The VTA-ALIC tract was built using the left/right VTA and the corresponding left/right ALIC as regions of interest (ROIs). The tracking parameters were kept the same as the whole brain tractography. The VTA was extracted from automated anatomical labelling atlas 3 and the ALIC was extracted from the JHU ICBM-DTI-81 White-Matter atlas. The VAT built in MNI space was transformed into the patient-specific coordinate system as the tracts. Each tract contained several fibres. The minimum perpendicular distance from the centre of gravity of the VAT to the fibres was calculated per tract. The median was then used as the distance to the centre of the tract for each VAT. Only the distance to the tracts on the same side was analysed.

Connectome construction and graph analysis

MRtrix V.3 software was used for the construction of the structural connectome. Preprocessing of diffusion images included denoising, removal of Gibbs ringing artefacts and the use of the FSL toolbox[21] to correct for distortions induced by susceptibility off-resonance fields, eddy currents and head motion. Fibre orientation densities were generated by multishell, multitissue constrained spherical deconvolution method and were subsequently normalised to obtain quantitative measures of density. T1-weighted images of each subject were registered to the mean b=0 image after preprocessing of DWI images. Anatomical images were coregistered with the standard space using ANTs to transform the AAL90 template to subject space. Brain tissue information was estimated from all T1-weighted images to obtain image segmentations of GM, sub GM, WM and cerebral spinal fluid using FSL. A total of 10 million probabilistic streamlines were generated using Second-order Integration over Fibre Orientation Distributions and Anatomically Constrained Tractography framework.[28] The initial tractogram was generated with 10 million streamlines using the default settings and the Spherical-deconvolution Informed Filtering of Tractograms (SIFT) methodology was applied to filter the streamlines to 1 million. The tcksift2 method was adopted to compute the streamline weights that were designed to reduce known biases in tractography data.[29] Finally, the SIFT2-weighted connections divided by the sum of the GM volume of two node regions were calculated to generate the undirected 90×90 weighted matrices.

The matrices were analysed by the Graph Theory Network Analysis toolbox.[30] Binary connection matrices were generalised with a sparse threshold of 30%. Node metrics included betweenness centrality, degree centrality, nodal efficiency, nodal clustering coefficient, nodal local efficiency and nodal shortest path. Global metrics included network global efficiency, local efficiency and small-world indexes including clustering coefficient, characteristic path length, normalised clustering

coefficient (γ), normalised shortest path length and small-world property (σ). The false discovery rate (FDR) correction was used for the comparison of multiple brain regions between the two groups in node parameters. Age was used as a covariate in the analysis.

Statistical analysis

Data were first tested for distribution using the Kolmogorov-Smirnov test, and then parametric (paired two-sample t-test or Pearson's correlation coefficient) or non-parametric (paired Wilcoxon rank-sum test or Spearman's correlation coefficient) statistic was used to assess potential differences or correlation of continuous variables. χ^2 fisher exact test was used to compare categorical variables between groups. Variables included age, gender, employment status, marriage status, years of education, disease duration as well as multiple psychiatric scales scored at baseline. Pearson/Spearman's partial correlation coefficients were calculated in the correlation analysis of fibre bundle properties (FA, MD, AD, RD, NQA) with HAMD-17 improvement considering age as a covariate. The FDR correction was used in graph analysis. Two-tailed p value <0.05 was considered significant. Statistical data were presented as mean (SD).

RESULTS
Baseline characteristics and clinical outcomes

Among the 14 patients included in the study, the mean improvement in HAMD-17 scores was 41.4% (SD=30.4%) at the 6-month follow-up. Three patients achieved remission, defined as a reduction in HAMD-17 scores to ≤7. Additionally, five patients (5/14) experienced a >50% improvement in HAMD-17 scores, indicating clinical response (table 1). The average number of times for parameter adjustments within 6 months was 8.0 (SD=7.3).

When correlating baseline characteristics with HAMD-17 improvements, associations were found in the depression severity measured by HAMD-17, MARDS and self-reported DSSS scale, anxiety measured by HAMA-14, social life impairments measured by SDS, attention impulsiveness measured by BIS-11, vitality measured by SF-36 and anhedonia measured by DARS scale. Significant differences were also observed in the items of depression, anxiety, anhedonia, attention impulsiveness severity and social life impairments between the remission and non-remission groups (online supplemental tables 1 and 2).

WM features

In the TBSS analysis, no significant clusters of FA, MD, AD, RD and NQA differences were observed between the response/non-response and remission/non-remission groups. In the analysis of fibre bundle properties, the FA, MD and RD values of left superior thalamic radiation were found to be significantly different between groups, with the FA value being statistically higher and the MD and RD values statistically lower in the remission group (FA: p=0.008, t=3.19, MD: p=0.012, t=2.94, RD: p=0.013, t=2.93,

Table 1 Characteristics of included patients and the clinical scales at baseline and 6-month follow-up

Items	Baseline (SD)	6-month follow-up	Statistic value
Gender	1F/13M	/	/
Age (years)	31.5 (6.6)	/	/
Duration of disease (years)	14.1 (6.2)	/	/
Years of education	12.9 (3.3)	/	/
MoCA	26.8 (2.3)	/	/
HAMA-14	23.7 (7.8)	14.6 (8.0)	t=4.76, p<0.001
HAMD-17	21.4 (3.6)	12.9 (7.1)	t=5.46, p<0.001
MADRS	30.4 (6.7)	18.9 (9.7)	t=5.07, p<0.001

F, female; HAMA-14, Hamilton anxiety rating scale; HAMD-17, 17-item Hamilton depression rating scale; M, male; MADRS, Montgomery-Asberg Depression Rating Scale; MoCA, Montreal Cognitive Assessment.

figure 2). The FA and RD values of the right reticulospinal tract (FA: p=0.009, t=3.10, RD: p=0.038, t=2.33) and the right parahippocampal parietal cingulum (FA: p=0.036, t=2.36, RD: p=0.038, t=2.33) were different between the remission and non-remission groups, with the FA value being significantly higher and the RD value significantly lower in the remission group. In the correlation analysis, the FA, MD and RD values of left superior thalamic radiation correlated with the HAMD-17 improvement after the correction of age (FA: p=0.003, r=0.75, MD: p=0.010, r=–0.67, RD: p=0.006, r=–0.72). No combined changes in fibre bundle properties were observed between the response and non-response groups.

In the analysis of fibre tracts traversing the individual VAT, anterior thalamic radiation is the major component in the fibre tracts (figure 2). Significant differences in the percentage of fibre tracts going through the VAT were found in the left superior thalamic radiation between the remission and non-remission groups (p=0.033, t=2.44) and in the right corticopontine tract frontal between the response and non-response groups (p=0.036, t=2.36). The FA, MD and RD values of the left anterior thalamic radiation (FA: p=0.014, t=2.86, MD: p=0.022, t=2.62, RD: p=0.018, r=2.75) and the left superior thalamic radiation (FA: p=0.013, t=2.95, MD: p=0.011, t=3.04, RD: p=0.008, t=3.25), as well as the FA and RD values of the right anterior thalamic radiation (FA: p=0.041, t=2.30, RD: p=0.016, t=2.79) were found to be different between the remission and non-remission groups (online supplemental tables 3–9). Differences in the FA and RD values of right anterior thalamic radiation were also observed between the response and non-response groups (FA: p=0.011, t=3.00, RD: p=0.012, t=2.97).

Distance estimation
We estimated the distance of the centre of each VAT to the centre of corresponding anterior thalamic radiation and tracts connecting VTA and ALIC (VTA-ALIC) on the same side (figure 3). No significant correlations were found between the distance of the centre of the VAT to any fibre tracts evaluated and the HAMD-17 improvements. The MNI X coordinate on the left negatively correlated with the HAMD-17 improvements (p=0.003, r=–0.74). When comparing the remission and non-remission groups, a significant difference in the distance to the left VTA-ALIC tract was observed (p=0.010, t=3.07). A tendency of difference in the distance to the right VTA-ALIC tract (p=0.054, t=2.14) was also observed. Centres of the VAT in the remission group had a significantly closer distance to the left VTA-ALIC tracts than the non-remission group (figure 3, table 2). Significant differences were also observed in the left and right MNI X coordinates between the remission and non-remission groups. No significant difference in the distance was observed between the response and non-response groups.

Graph analysis
No significant difference was observed in the edges and nodes in the structural connectome between the response/non-response and remission/non-remission groups. Nevertheless, global metrics including the normalised clustering coefficient (γ) and the small-world property (σ) were both statistically higher in the remission group compared to the non-remission group (γ: p=0.048, t=2.22, σ: p=0.044, t=2.27, figure 3). The difference was also observed between the response and non-response groups (γ: p=0.007, t=3.33, σ: p=0.008, t=3.25). The γ and σ also correlated with the symptom improvement after the correction of age (γ: p=0.006, r=0.72, σ: p=0.011, r=0.68).

DISCUSSION
Main findings
This study correlated baseline characteristics and presurgical structural imaging to identify potential biomarkers associated with the individual outcome of the combined BNST–NAc DBS. Patients with more severe depression symptoms, including anhedonia, lack of vitality, increased attention impulsiveness and anxiety, tend to benefit less from the DBS treatment. Among the analysis of fibre bundle properties and graph indexes, fibre features in tracts including superior thalamic radiation and reticulospinal tract, graph indexes including
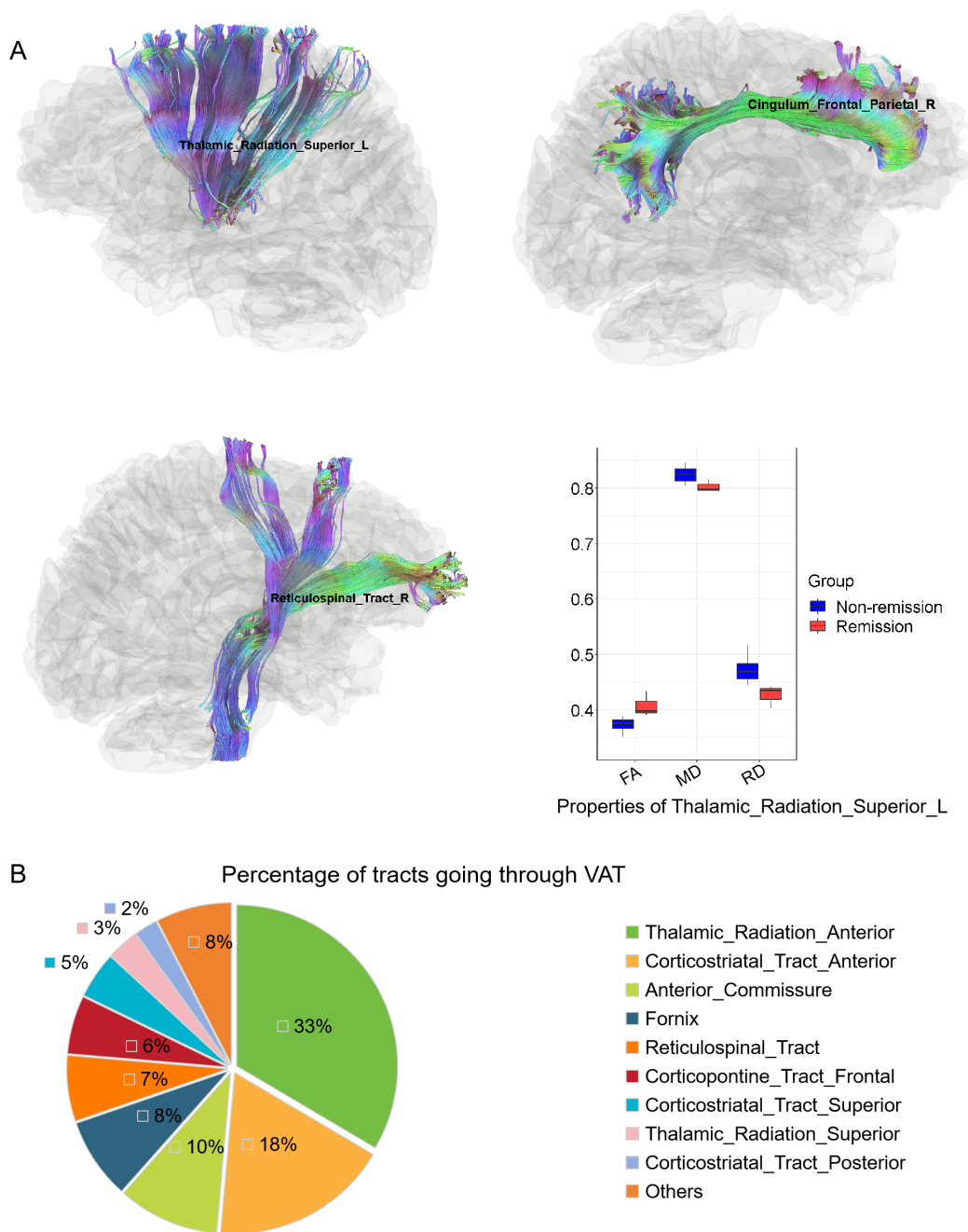
Figure 2 Tracts with significant difference in fibre bundle properties and the component of tracts traversing the volume of activated tissue. (A) Tracts with significant differences in fibre bundle properties between the remission and non-remission groups. (B) Percentage of fibre tracts that traverse the volume of activated tissue. VAT, volume of activated tissue.

the small world property and the normalised clustering coefficient in the structural connectome were identified to correlate with the clinical outcome. Besides, we found that distance of the centre of the VAT estimated by stimulation parameters to the tract connecting the VTA-ALIC varied between the remission and non-remission groups. The findings from structural imaging indicated the influence of the individual structural alterations on DBS modulation, providing clues for the prediction of individual outcomes after DBS surgery in patients with TRD.

Our study replicated previous findings that WM integrity of fibre tracts connecting the frontal cortex with subcortical regions affected the efficacy of DBS.[9] The associations were observed in fibre bundles including thalamic radiation and the reticulospinal tract. Decreased FA and increased MD and RD values were shown in the tracts in the non-remission group. The fibre bundle properties were strongly associated with the demyelination of the fibre tracts.[31] Physiology studies have found that poorly myelinated fibres fail to transmit consecutive antidromic spikes
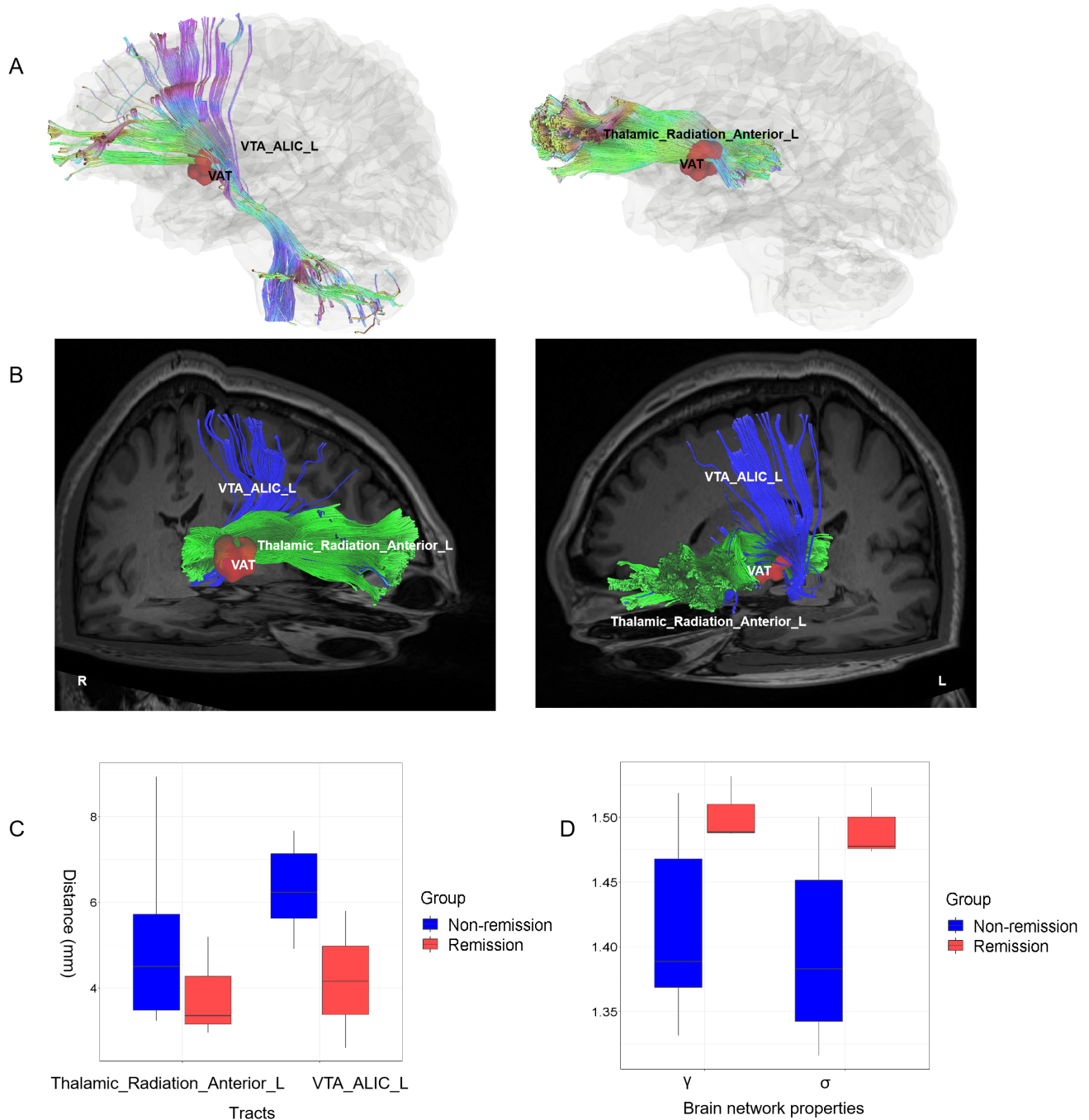
Figure 3 Tracts and their relative positions with VAT and the difference of indexes in graph analysis. (A) Illustration of the VTA-ALIC tract and the anterior thalamic radiation. (B) The relative position of the volume of activated tissue and the specific fibre tracts. (C) Distance to the left VTA-ALIC tracts and the left anterior thalamic radiation between the remission and non-remission groups. (D) Differences in the normalised clustering coefficient (γ) and the small-world property (σ) between the remission and non-remission groups. ALIC, anterior limb of internal capsule; VAT, volume of activated tissue; VTA, ventral tegmental area.

at the start of DBS, suggesting antidromic excitation is strongly influenced by the myeloarchitecture.[32] In a diffusion tensor imaging-functional MRI study, increased integrity of WM in the ALIC region was positively correlated with reward-related activation in the NAc, indicating that the microstructural integrity of fibre tracts may influence the intensity of reward-related responsiveness of the ventral striatum.[33] Changed fibre properties may restrain information

transfer in the brain network, thereby impairing the modulatory effect of DBS. Differences in the brain network were indeed observed in graph analysis. Although our intention to find potential edges that correlate with clinical improvements yielded no significant findings, the small world property and the normalised clustering coefficient did correlate with HAMD-17 improvement, which demonstrated that network efficiency of the brain and its balance with

Table 2 Coordinates of the volume of activated tissue and their distance to specific fibre tracts

Items	Non-remission	Remission	Statistic value
MNIX_L	−7.47 (0.31)	−10.42 (0.92)	p=0.002, t=3.98
MNIY_L	4.06 (1.13)	2.36 (2.63)	p=0.104, t=1.76
MNIZ_L	−1.62 (3.72)	3.26 (3.51)	p=0.064, t=2.04
MNIX_R	8.66 (0.51)	11.03 (0.36)	p=0.040, t=2.31
MNIY_R	3.66 (1.63)	2.44 (1.06)	p=0.252, t=1.20
MNIZ_R	−1.06 (3.22)	1.50 (1.56)	p=0.216, t=−1.31
Distance to the left anterior thalamic radiation	7.50 (2.74)	5.75 (1.79)	p=0.323, t=1.03
Distance to the left VTA-ALIC	9.48 (1.38)	6.28 (2.39)	p=0.010, t=3.07
Distance to the right anterior thalamic radiation	4.31 (1.66)	2.51 (0.60)	p=0.097, t=1.80
Distance to the right VTA-ALIC	7.63 (1.73)	5.42 (0.58)	p=0.054, t=2.14

ALIC, anterior limb of internal capsule; VTA, ventral tegmental area.

local specialisations had an impact on the effect of DBS surgery.

The anterior thalamic radiation and slMFB were reported to be the main fibre tracts that mediated the effect of DBS in the ALIC and nearby regions.[26] Previous studies showed that stimulation in the ALIC closer to both tracts correlated with symptom alleviation.[27] Our target, compared with the previous one, was located more ventrally and medially, reaching more areas in the NAc and BNST nuclei. Nevertheless, according to the results of our study, a relatively lateral position of the VAT centre on the left was associated with better clinical outcomes. This can be explained, at least partially, by the modulation of fibre bundles, as our tracking shows that a more lateral position of the VAT tends to activate more fibres connecting VTA-ALIC, which are located more laterally than the anterior thalamic radiation in the level of stimulation in the brain.[34] Notably, in the previous study, the significant correlation was not observed until the duration of chronic stimulation after the optimisation of stimulation parameters was used as a covariate, suggesting the duration of stimulation may be an influential factor.[27] A longitudinal analysis considering its effect may help further clarify the issue.

Limitations

Various factors may influence the clinical outcome of patients with TRD, including the duration of the stimulation, the adjustment of the parameters and the placebo effect. The restriction of deterministic fibre tracking with automated recognition of tracts based on atlas, the single-centre experience as well as the limited number of patients can influence the generalisability of our analysis. A double-blinded randomised clinical trial is currently underway to rule out the placebo effect. Fibre tracking with more focus on specific tracts and ROIs may provide further insights into the mechanisms of DBS modulation.

Implications

Presurgical structure alterations in patients with TRD can influence the outcome of the combined BNST–NAc DBS. Fibre tracts connecting the frontal area with subcortical regions, the small world property and the normalised clustering coefficient of the brain network are correlated with the DBS outcome. Distance to the VTA-ALIC tract also influences the modulatory effects. These findings shed light on the regulatory mechanisms of DBS and can inform presurgical planning for the treatment of TRD. Future studies incorporating electrophysiology analysis may further elucidate the complexity of DBS modulation in patients with TRD.

Author affiliations
[1]Department of Neurosurgery, Shanghai Jiao Tong University Medical School Affiliated Ruijin Hospital, Shanghai, China

[2]Department of Psychiatry, Zhejiang University School of Medicine Sir Run Run Shaw Hospital, Hangzhou, China

[3]Fudan University Institute of Science and Technology for Brain-inspired Intelligence, Shanghai, China

[4]Clinical Research Center for Mental Disorders, Shanghai Pudong New Area Mental Health Center, Shanghai, China

[5]Department of Psychiatry, University of Cambridge, Cambridge, UK

ORCID iDs
Fengting Wang http://orcid.org/0000-0002-6693-3140
Yijie Lai http://orcid.org/0000-0003-4443-0136

REFERENCES

1 Rush AJ, Warden D, Wisniewski SR, *et al*. STAR*D: revising conventional wisdom. *CNS Drugs* 2009;23:627–47.
2 Figee M, Riva-Posse P, Choi KS, *et al*. Deep brain stimulation for depression. *Neurotherapeutics* 2022;19:1229–45.
3 Zhu Z, Hubbard E, Guo X, *et al*. A connectomic analysis of deep brain stimulation for treatment-resistant depression. *Brain Stimul* 2021;14:1226–33.
4 Ruan H, Wang Y, Li Z, *et al*. A systematic review of treatment outcome predictors in deep brain stimulation for refractory obsessive-compulsive disorder. *Brain Sci* 2022;12:936.
5 Huang L-C, Chen L-G, Wu P-A, *et al*. Effect of deep brain stimulation on brain network and white matter integrity in Parkinson's disease. *CNS Neurosci Ther* 2022;28:92–104.
6 Coenen VA, Schlaepfer TE, Bewernick B, *et al*. Frontal white matter architecture predicts efficacy of deep brain stimulation in major depression. *Transl Psychiatry* 2019;9:197.
7 Clark DL, Johnson KA, Butson CR, *et al*. Tract-based analysis of target engagement by Subcallosal cingulate deep brain stimulation for treatment resistant depression. *Brain Stimul* 2020;13:1094–101.
8 Liao Y, Huang X, Wu Q, *et al*. Is depression a disconnection syndrome? Meta-analysis of diffusion tensor imaging studies in patients with MDD. *J Psychiatry Neurosci* 2013;38:49–56.
9 Wang T, Dai L, Lai Y, *et al*. Parameter-based analysis of clinical efficacy of combined bed nucleus of the stria terminalis-nucleus accumbens deep brain stimulation for treatment-resistant depression. *J Neurosurg* 2024;12 2024:1–11.
10 Lai Y, Dai L, Wang T, *et al*. Structural and functional correlates of the response to deep brain stimulation at ventral capsule/ventral striatum region for treatment-resistant depression. *J Neurol Neurosurg Psychiatry* 2023;94:379–88.
11 Zheng YP, Zhao JP, Phillips M, *et al*. Validity and reliability of the Chinese Hamilton Depression Rating Scale. *Br J Psychiatry* 1988;152:660–4.
12 Liu J, Xiang Y-T, Lei H, *et al*. Guidance on the conversion of the Chinese versions of the Quick Inventory of Depressive Symptomatology-Self-Report (C-QIDS-SR) and the Montgomery–Asberg Scale (C-MADRS) in Chinese patients with major depression. *J Affect Disord* 2014;152–154:530–3.
13 Leung CM, Wing YK, Kwong PK, *et al*. Validation of the Chinese-Cantonese version of the Hospital Anxiety and Depression Scale and comparison with the Hamilton Rating Scale of Depression. *Acta Psychiatr Scand* 1999;100:456–61.
14 Tse PS, González DA, Jenkins SR. Validating the structure of the depression and somatic symptoms scale. *Psychosomatics* 2018;59:277–82.
15 Liu J, Xiang Y-T, Wang G, *et al*. Psychometric properties of the Chinese versions of the Quick Inventory of Depressive Symptomatology - Clinician Rating (C-QIDS-C) and Self-Report (C-QIDS-SR). *J Affect Disord* 2013;147:421–4.
16 Zeljic K, Zhang Y, Qiu X, *et al*. An evaluation of the psychometric properties of the Sheehan Disability Scale in a Chinese psychotherapy-seeking sample. *J Cogn Psychother* 2020;34:58–69.
17 Lin Y, Yu Y, Zeng J, *et al*. Comparing the reliability and validity of the SF-36 and SF-12 in measuring quality of life among adolescents in China: a large sample cross-sectional study. *Health Qual Life Outcomes* 2020;18:360.
18 Lu CF, Jia CX, Xu AQ, *et al*. Psychometric characteristics of Chinese version of Barratt Impulsiveness Scale-11 in suicides and living controls of rural China. *Omega (Westport)* 2012;66:215–29.
19 Xiao W-Y, Zhu R-Z, Lv Z-X, *et al*. Psychometric properties of the dimensional Anhedonia rating scale in Chinese typical, subthreshold, and clinically depressed adolescents. *Psych J* 2022;11:344–55.
20 Horn A, Kühn AA. Lead-DBS: a toolbox for deep brain stimulation electrode localizations and visualizations. *Neuroimage* 2015;107:127–35.
21 Smith SM, Jenkinson M, Woolrich MW, *et al*. Advances in functional and structural MR image analysis and implementation as FSL. *Neuroimage* 2004;23 Suppl 1:S208–19.
22 Yeh F-C, Wedeen VJ, Tseng W-YI. Generalized q-sampling imaging. *IEEE Trans Med Imaging* 2010;29:1626–35.
23 Yeh F-C, Verstynen TD, Wang Y, *et al*. Deterministic diffusion fiber tracking improved by quantitative anisotropy. *PLoS One* 2013;8:e80713.
24 Yeh F-C, Panesar S, Fernandes D, *et al*. Population-averaged atlas of the macroscale human structural connectome and its network topology. *Neuroimage* 2018;178:57–68.
25 Smith SM, Jenkinson M, Johansen-Berg H, *et al*. Tract-based spatial statistics: voxelwise analysis of multi-subject diffusion data. *Neuroimage* 2006;31:1487:1487–505:.
26 Coenen VA, Panksepp J, Hurwitz TA, *et al*. Human medial forebrain bundle (MFB) and anterior thalamic radiation (ATR): imaging of two major subcortical pathways and the dynamic balance of opposite affects in understanding depression. *J Neuropsychiatry Clin Neurosci* 2012;24:223–36.
27 Liebrand LC, Natarajan SJ, Caan MWA, *et al*. Distance to white matter trajectories is associated with treatment response to internal capsule deep brain stimulation in treatment-refractory depression. *Neuroimage Clin* 2020;28:102363.
28 Smith RE, Tournier JD, Calamante F, *et al*. Anatomically-constrained tractography: improved diffusion MRI streamlines tractography through effective use of anatomical information. *Neuroimage* 2012;62:1924–38.
29 Smith RE, Tournier J-D, Calamante F, *et al*. Sift2: enabling dense quantitative assessment of brain white matter connectivity using streamlines tractography. *Neuroimage* 2015;119:338–51.

30 Wang J, Wang X, Xia M, *et al*. GRETNA: a graph theoretical network analysis toolbox for imaging connectomics. *Front Hum Neurosci* 2015;9:386.

31 Alexander AL, Lee JE, Lazar M, *et al*. Diffusion tensor imaging of the brain. *Neurotherapeutics* 2007;4:316–29.

32 Chomiak T, Hu B. Axonal and somatic filtering of antidromically evoked cortical excitation by simulated deep brain stimulation in rat brain. *J Physiol* 2007;579:403–12.

33 Koch K, Wagner G, Schachtzabel C, *et al*. Association between white matter fiber structure and reward-related reactivity of the ventral striatum. *Hum Brain Mapp* 2014;35:1469–76.

34 Coenen VA, Schumacher LV, Kaller C, *et al*. The anatomy of the human medial forebrain bundle: ventral tegmental area connections to reward-associated subcortical and frontal lobe regions. *Neuroimage Clin* 2018;18:770–83.

Fengting Wang obtained her bachelor degree of science from School of Pharmacy, Shanghai Jiao Tong University and her MD degree in neurosurgery from Shanghai Jiao Tong University School of Medicine, China in June, 2023. She has been a resident doctor and postdoc in the department of functional neurosurgery in Ruijin Hospital, Shanghai, China, since August 2023. Her main research interests include predictions of efficacy of deep brain stimulation (DBS) in psychiatric and movement disorders as well as the modulating mechanisms of DBS and MR-guided focused ultrasound. Her work in NPJ Parkinson's disease recapitulated brain morphometric findings that predict the outcome of DBS in Parkinson's disease. Her collaborating work in Journal of Neurology, Neurosurgery and Psychiatry delineated a frontothalamic pathway and connectivity profile responsive for clinical outcome of DBS for treatment-resistant depression.